

CONNECTIONS BETWEEN LOCAL AND GLOBAL TURBULENCE IN ACCRETION DISKS

KAREEM A. SORATHIA^{1,3}, CHRISTOPHER S. REYNOLDS^{2,3}, PHILIP J. ARMITAGE^{4,5}

Draft version October 30, 2018

ABSTRACT

We analyze a suite of global magnetohydrodynamic (MHD) accretion disk simulations in order to determine whether scaling laws for turbulence driven by the magnetorotational instability, discovered via local shearing box studies, are globally robust. The simulations model geometrically-thin disks with zero net magnetic flux and no explicit resistivity or viscosity. We show that the local Maxwell stress is correlated with the self-generated local vertical magnetic field in a manner that is similar to that found in local simulations. Moreover, local patches of vertical field are strong enough to stimulate and control the strength of angular momentum transport across much of the disk. We demonstrate the importance of magnetic linkages (through the low-density corona) between different regions of the disk in determining the local field, and suggest a new convergence requirement for global simulations – the vertical extent of the corona must be fully captured and resolved. Finally, we examine the temporal convergence of the average stress, and show that an initial long-term secular drift in the local flux-stress relation dies away on a time scale that is consistent with turbulent mixing of the initial magnetic field.

Subject headings: accretion, accretion disks — instabilities — MHD — turbulence

1. INTRODUCTION

The modern theory of accretion disks has been dominated by the discovery that angular momentum transport can be mediated by magnetohydrodynamic (MHD) turbulence driven by the magnetorotational instability (MRI; Balbus & Hawley 1991, 1998). Although analytic treatments of the MRI suffice to establish that the instability exists and rapidly develops toward turbulence, numerical work has been at the forefront of the effort to characterize the resulting angular momentum transport. Simulations of the MRI require difficult compromises because arguably important scales span a wide range between the global scale $\lambda \sim r$, an intermediate scale $\lambda \sim h$ (where h is the disk scale height) that roughly defines the scale over which shear dominates turbulent fluctuations, and viscous and resistive dissipation scales λ_ν and λ_η . As in many other astrophysical problems, the latter are usually so small that in the disks under consideration it is impossible to run simulations that capture the physical dissipative scales.

To date, the bulk of our numerical understanding of the MRI has been derived from local shearing-box simulations (Hawley et al. 1995; Brandenburg et al. 1995). In a local shearing-box model, one studies the local dynamics of an orbiting patch of the accretion flow using a (co-rotating) Cartesian coordinate system by including Coriolis forces and shearing boundary conditions. Since only a small patch of the disk is being simulated, this

approach maximizes the separation between the intermediate driving scale of the turbulence and the dissipative scales. For our purposes, the result that in local simulations the saturation level of magnetic fields and the strength of angular momentum transport are found to scale with the vertical flux threading the simulation domain (Hawley et al. 1995; Sano et al. 2004; Pessah et al. 2007) will be of particular interest.

Local simulations have known limitations (Regev & Umurhan 2008; Bodo et al. 2008). By construction, they enforce the local conservation of quantities (in particular the net magnetic flux) that in reality are only globally conserved. In many older implementations they also enforce periodicity (in radius, azimuth, and in some instances also height) on a scale that may be small enough to impact the results. Recently, a number of authors (Davis et al. 2009; Guan et al. 2009; Johansen et al. 2009) have used larger than usual shearing-box simulations to quantify whether these limitations matter for practical purposes. In this paper we address the same problem from the other direction. We analyze small patches of *global* disk simulations in an attempt to determine whether the disk behaves as if it were a collection of shearing-boxes. Our specific goal is to ascertain whether the relationship between local $r\phi$ -component of the magnetic stress and vertical magnetic flux that is found in local simulations (Pessah et al. 2007) is recovered in local patches of global simulations. As a result, we uncover the importance of the magnetic connectivity of the disk and the need to fully capture the vertical extent of the corona.

This paper is organized as follows. §2 briefly describes the global simulations that we employ. §3.1 describes the vertical structure of the disks we simulate with an emphasis on the distribution of magnetic flux. We discuss, in Section §3.2, the results of our study of instantaneous correlations between magnetic flux and stress. The flux-stress connection is explored in more detail in Sec-

¹ Department of Mathematics and Department of Astronomy, University of Maryland, College Park, MD 20742-2421

² Department of Astronomy and the Maryland Astronomy Center for Theory and Computation, University of Maryland, College Park, MD 20742-2421

³ Joint Space Science Institute (JSI), University of Maryland, College Park, MD 20742-2421

⁴ JILA, 440 UCB, University of Colorado, Boulder, CO 80309-0440

⁵ Department of Astrophysical and Planetary Sciences, University of Colorado, Boulder, CO 80309-0391

tion §3.3 (where we discuss the nature of the transition point in the flux-stress relation) and Section §3.4 (where we examine the temporal correlation of stress and vertical flux in co-moving patches). Sections §3.5 and §3.6 describe the dependence of angular momentum transport on vertical domain size and time respectively. Section §4 presents our conclusions.

2. GLOBAL SIMULATIONS OF THIN ACCRETION DISK

The simulations used here are very similar to those described by Reynolds & Miller (2009). We use the ZEUS-MP code (Stone & Norman 1992; Hayes et al. 2006) to solve the equations of ideal MHD in three dimensions. We modified the basic version of the code to incorporate a Paczynski-Wiita pseudo-Newtonian gravitational potential (as a first approximation of the gravitational field about a Schwarzschild black hole; Paczynski & Wiita 1980) and performed the simulation in cylindrical polar coordinates. Our simulations are ideal MHD in the sense that no explicit resistive or viscous dissipation is included; all dissipative processes are due to the discretization of the spatial domain and hence occur close to the grid scale. Furthermore, we integrate an internal energy equation assuming an adiabatic equation of state with $\gamma = 5/3$. Energy is lost from the domain when magnetic fields undergo numerical reconnection.

The initial disk is in a state of Keplerian rotation (with respect to the pseudo-Newtonian potential), and is in vertical hydrostatic equilibrium with a constant scale-height h . Thus, the initial density, pressure and velocity field is

$$\rho(r, z) = \rho_0(r) \exp\left(-\frac{z^2}{2h^2}\right), \quad (1)$$

$$p(r, z) = \frac{GMh^2}{(R - 2r_g)^2 R} \rho(r, z), \quad (2)$$

$$v_\phi = r\Omega = \frac{\sqrt{GMr}}{r - 2r_g}, \quad v_z = v_r = 0, \quad (3)$$

where r represents the cylindrical radius, $R = \sqrt{r^2 + z^2}$, $r_g = GM/c^2$ and $h = 0.05r_{isco} = 0.3r_g$. We set the initial midplane density to be $\rho_0(r) = 1$ beyond the innermost stable circular orbit (ISCO) at $r_{isco} = 6r_g$, and $\rho_0(r) = 0$ within the ISCO. The radial boundary conditions correspond to zero-gradient outflow, while periodic boundaries were imposed on both the ϕ and z -boundaries (this last choice, which is made in order to avoid field-line snapping and other numerical problems, is discussed further in Reynolds & Miller 2009).

The initial magnetic field is specified in terms of a vector potential of the form,

$$A_\phi = A_0 f(r, z) p^{1/2} \sin\left(\frac{2\pi r}{5h}\right), \quad (4)$$

$$A_r = A_z = 0. \quad (5)$$

Here f is an envelope function that is unity in the disk body and smoothly goes to zero away from the main body so as to avoid unphysical interactions with the boundaries. This results in a magnetic field topology consisting of distinct poloidal field loops of alternating orientation throughout the main body of the simulation. Of importance to the current discussion is that there is no

net vertical magnetic flux threading the disk as a whole. The constant A_0 is chosen to ensure that the magnetic field strength is normalized so that the ratio of volume-integrated gas and magnetic pressure $\beta \approx 10^3$.

A set of simulations were run to span a range of numerical parameters, specifically varying the vertical and radial resolution, as well as the vertical and azimuthal extent of the domain. A comparison of simulations with varying azimuthal extents suggest a negligible dependence on this parameter, and as such all the simulations considered here use the same 30° wedge-shaped azimuthal domain. The vertical domain size was found to be important, and we will discuss the role of this parameter later in this paper. A detailed study of the dependence on resolution, requiring much greater computational expense, is deferred to a later work. All simulations presented here have a radial domain $r \in (4r_g, 16r_g)$. Details of the simulations considered are given below in Table 1.

3. RESULTS

3.1. Vertical Structure of Thin Disks

Our primary goal is to study the instantaneous correlation between stress and magnetic flux within the simulated disk. In a stratified disk this correlation may vary with height above the disk midplane, and hence we start by considering how the mean magnetic field structure varies vertically in our simulations.

To analyze the simulations the principle quantity of interest is the $r - \phi$ component of the Maxwell stress tensor,

$$M_{r\phi} = \frac{B_r B_\phi}{4\pi}, \quad (6)$$

which dominates MRI-driven angular momentum transport (Balbus & Hawley 1998). In a turbulent disk, both $M_{r\phi}$ and other physical quantities of interest are complicated functions of space and time. To make sense of them we use temporal and spatial averages. Run `Thin.M-Res.6z` has the longest duration of any of our simulations, and we use this run to construct a representative vertical profile of the magnetic structure of the disk. To reduce the effects of spatial intermittency in the turbulence, we azimuthally average over the entire domain and average over a small radial range centered about a fiducial radius in the body of the disk ($8r_g - h < r < 8r_g + h$). To smooth out the temporal variability and isolate the behavior of the disk in a saturated turbulent state we time average over 400 ISCO orbits starting at orbit 50.

The results are given in Figure 1, which shows the vertical profiles of the relevant quantities scaled to their maximum values. Our interest in vertical structure is predominantly in the magnetic fields, and in particular the vertical magnetic flux, B_z , and the magnetic stress, $M_{r\phi}$. However, we also plot the density, ρ , to highlight the contrast between the relatively unmagnetized midplane of the disk and the sparse magnetized ‘‘corona’’ away from the midplane. The obvious reason for the formation of these two disparate regions is magnetic buoyancy resulting from the effect of vertical gravity, but this may be overly simplistic. Also of interest is the double-peak vertical profile of vertical flux and stress. Broadly similar results are seen in a subset of the stratified lo-

Run ID	Resolution (R, ϕ, z)	Vertical Extent (in r_g)	Total Orbits (at r_{isco})	Mean α_M	Standard Deviation of α_M
Thin.M-Res.12z	(240,32,512)	12	122	0.008	0.0011
Thin.M-Res.6z	(240,32,256)	6	664	0.0086	0.0016
Thin.M-Res.3z	(240,32,128)	3	112	0.0061	0.001

TABLE 1

THE SPATIAL RESOLUTION, VERTICAL DOMAIN SIZE, DURATION OF THE SIMULATIONS ANALYZED IN THIS WORK. ALSO INCLUDED ARE THE MEAN AND STANDARD DEVIATION OF α_M , DEFINED BY EQUATION 14, BETWEEN 50 AND 100 ORBITS AT r_{isco} .

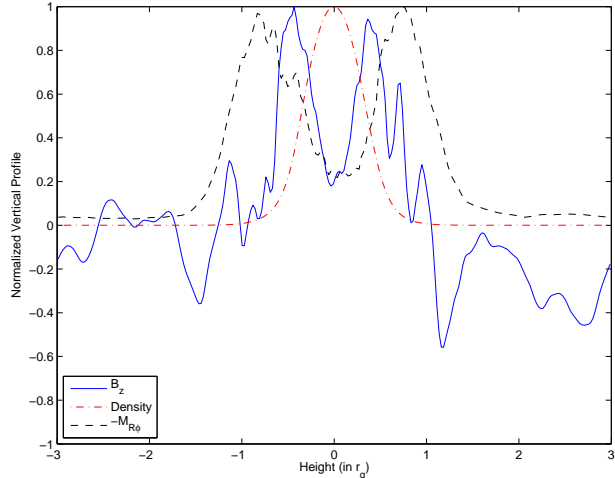


FIG. 1.— Vertical structure of physical quantities averaged over four hundred orbits for run **Thin.M-Res.6z**.

cal simulations of Miller & Stone (2000) and a subset of the global simulations of Fromang & Nelson (2006). It is interesting that the vertical location of the peak field and stress seem to approach constant values rather than growing monotonically with time. Whether the region of strong flux is trapped, possibly due to magnetic tension from field lines connecting it to the midplane, or is continually dissipating while outflowing, is currently unclear.

The local flux-stress relationship we will compare our results to is based on unstratified shearing box simulations and the rich vertical magnetic structure due to stratification in our global disk means that there is necessarily some ambiguity in the comparison. In what follows, we therefore analyze the flux-stress relationship within the global simulation not just at the midplane but also as a function of height. One should note that the offset of the peak vertical flux and stress from $z = 0$ means that high values of flux and stress are only accessible away from the midplane.

3.2. A local flux-stress correlation in a global disk

Although our simulations have zero net vertical flux, small patches of the disk *are* instantaneously threaded by a vertical field. We seek to determine whether the Maxwell stress tracks this transient vertical field in the same way as it would in a local simulation where the vertical field is persistent (Hawley et al. 1995; Pessah et al. 2007). To proceed, we break up the global simulation domain at each timestep into several hundred small cylindrical wedges of size $\Delta z = \Delta r = h$ and $\Delta \phi \approx 0.1$. Within each wedge we average to obtain a single estimate of the magnetic stress ($M_{r\phi}/p$, normalized to the local gas pressure) and the local vertical flux, which we express in

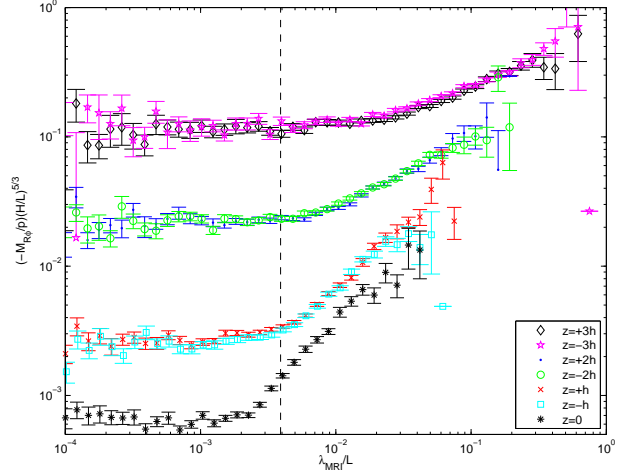


FIG. 2.— Flux versus stress averaged over four hundred orbits for run **Thin.M-Res.6z**.

terms of the wavelength of the most unstable MRI mode,

$$\lambda_{\text{MRI}} = 2\pi \left(\frac{16}{15} \right)^{1/2} \frac{\bar{v}_{Az}}{\Omega_0}, \quad (7)$$

where $v_{Az} = B_z/\sqrt{4\pi\rho}$ is the Alfvén speed corresponding to the vertical field component. Note that because we scale the stress by the local pressure (a decreasing function of height), we immediately introduce a height dependence. Choosing instead to scale by the midplane pressure (only a function of radius) still yields a height dependence and as such we are confident that the height dependence seen is not solely a consequence of the pressure scaling.

To avoid early transients, our analysis excludes the period prior to the first 50 ISCO orbital periods. To improve our statistics (and to give a measure of the convergence of our results given the finite duration of the run) we consider wedges that are centered at $z = \pm[0, 1, 2, 3]h$ and plot results for the samples separately. The resulting pairs of flux-stress values from all of the wedges and all of the snapshots in time were binned according to (logarithmic) vertical flux in order to diagnose trends.

The resulting flux-stress relations for all the simulations considered are broadly similar. Our best statistics come from the long duration run **Thin.M-Res.6z**, and the flux-stress relation for this case is plotted in Figure 2. The stress is observed to be flat for weak vertical fields (small λ_{MRI}), while for larger field strengths we have approximately $M_{r\phi} \propto \lambda_{\text{MRI}}$. This may be compared with the local scaling relation derived from unstratified simulations, which can be written in the form (Pessah et al.

2007),

$$\frac{-M_{r\phi}}{P} \left(\frac{H}{L}\right)^{(5/3)} = 0.61 \times \begin{cases} \Delta/L & : \lambda_{MRI} \leq \Delta, \\ \lambda_{MRI}/L & : \Delta < \lambda_{MRI} \leq L, \\ 0 & : L < \lambda_{MRI}, \end{cases} \quad (8)$$

where Δ and L are the vertical grid cell size and total box size respectively. The pressure scale height H is given by

$$H = \left(\frac{2}{\gamma}\right)^{1/2} \frac{c_s}{\Omega_0}, \quad (9)$$

where Ω_0 is the Keplerian angular velocity and c_s the sound speed. Note the distinction between the locally defined H and the globally constant h . In comparing our results to those obtained for local simulations, we consider L to be the size of the wedge and H to be the locally defined pressure scale height.

Our simulations do not spontaneously develop vertical fields strong enough to quench the MRI (and hence we do not sample the $\lambda_{MRI} > L$ regime), but the behavior of patches at low and intermediate vertical fluxes is qualitatively the same as that found in local simulations. In contrast to the local (unstratified) results of Pessah et al. (2007) is the strong dependence on height in our stratified simulations. In addition to the fact that the largest values of flux are only accessible at large heights is the fact that the stress response to flux is also height dependent. There is a height-dependence of the transition point between low and intermediate flux, as well as in the slope of the intermediate flux regime. Of particular note is the location of the transition point itself. The vertical line marked in Figure 2 is given by $\lambda_{MRI} = \Delta/20$, and approximately marks the location of the transition point at $z = \pm H$. This stands in contrast to the transition point for local unstratified simulations, $\lambda_{MRI} = \Delta_z$. We return to a discussion of the physics of this transition in Section 3.3.

The fact that transient self-generated vertical flux is able to stimulate the local stress in the same manner as occurs in local models is primarily a formal result, although it does lend some credence to models in which patches of vertical field are assumed to have a physical identity (Spruit & Uzdensky 2005). Of greater import is the observation that, across much of the disk, the self-generated field is strong enough to fall into the linear regime of the flux-stress relation. Figure 3 shows the distribution of flux through patches in all three. The vertical flux distributions are approximately symmetric in log-space. We find that, at any instant in time, about half of the area of the disk is threaded by a field strong enough to control the stress. We interpret this to mean that in a zero-net field global simulation, much of the disk sees a field strong enough to control its dynamics. In other words, the dynamics of the disk is strongly influenced by the connectivity of the self-generated magnetic field between different patches of the disk.

In these results we again see the importance of the magnetized region away from the midplane. Not only is this the location of the largest values of flux, and thus stress, but for the same flux the stress response is higher. This increased stress response to flux suggests that the corona is important not just as a warehouse of magnetic energy, but also has the ability to use this magnetic en-

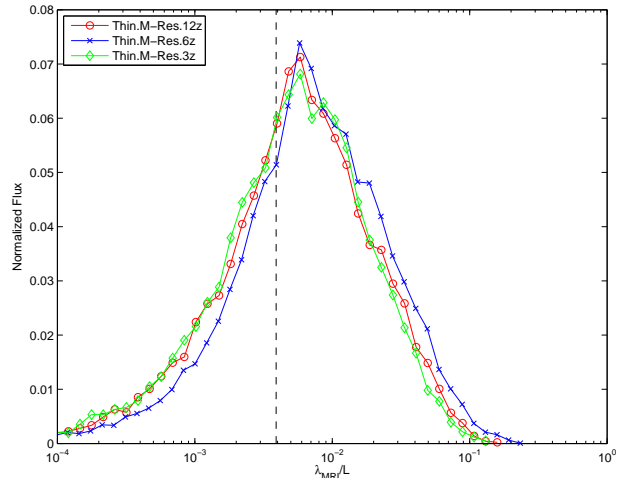


FIG. 3.— Normalized flux distributions for all simulations, computed between 50-100 ISCO orbits. The dashed vertical line indicates, approximately, the strength of vertical field above which magnetic stress in the disk is stimulated.

ergy more efficiently to induce angular momentum transport. One possible explanation for this efficiency is the ability of the corona to mediate magnetic links through radially disparate regions of the disk due to the presence of coronal field loops. In Section 3.5 we consider the effect of vertical domain size on the saturated turbulent stress as a means of diagnosing whether truncating the corona affects the dynamics of a disk. Before that, however, we discuss the nature of the transition point in the flux-stress relation as well as study the connection between the local vertical magnetic fields and stresses via their temporal correlation.

3.3. The nature of the transition point in the flux-stress relation

To reiterate, the flux-stress relation obtained from our global simulation shows a transition at approximately $\lambda_{MRI} \sim \Delta/20$, in contrast with $\lambda_{MRI} \sim \Delta$ found from local unstratified simulations (Pessah et al. 2007). Neither of these transitions can correspond straightforwardly to the condition that the fastest growing MRI mode is resolved. To resolve a mode in a ZEUS-like scheme requires that the wavelength is spanned by at least ~ 8 computational zones. Since λ_{MRI} is, by construction, the wavelength of the fastest growing mode corresponding to the net vertical magnetic field, the condition that the fastest growing MRI mode is resolved corresponds to $\lambda_{MRI} \sim 8\Delta$. Our result then implies that magnetic fields that are very weak – in the sense that their fastest growing mode cannot be resolved – nonetheless have an important influence on the dynamics of our global disk.

We do not have a quantitative explanation of why $\lambda_{MRI} \sim \Delta/20$. On general grounds, however, we note that we would expect that the transition point would lie at $\lambda_{MRI} \ll 8\Delta$. A given vertical field is unstable not just to the fastest growing mode, but also to a whole spectrum of slower-growing modes that have longer wavelengths that are more easily resolvable numerically. Plausibly, the transition point will then correspond to the condition that we resolve the slowest growing mode that grows appreciably before it is truncated by non-linear coupling

to other MRI modes or some other aspect of the physics (e.g. a dynamo cycle). If this is the case, then it is unsurprising that the transition point varies between local and global simulations, since the time scale available for a mode to grow may well depend on the presence or absence of a low density disk corona within which the MRI is not active.

To consider this more quantitatively, consider purely vertical MRI modes ($k_r = k_\phi = 0$) in a thin accretion disk (so that radial gradients of pressure and entropy can be neglected). Let the spacetime dependence of the modes be $e^{i(\omega t - kz)}$. The dispersion relation for these modes (Balbus & Hawley 1991) reads

$$\tilde{\omega}^4 - \kappa^2 \tilde{\omega}^2 - 4\Omega_0^2 k^2 v_A^2 = 0, \quad (10)$$

where $\tilde{\omega}^2 = \omega^2 - k^2 v_A^2$ and κ is the radial epicyclic (angular) frequency. We wish to examine modes with wavelengths much longer than the fastest growing mode, i.e., with $|k v_A / \Omega_0| \ll 1$. Rewriting in terms of the growth rate, $\sigma = -i\omega$ and expanding the dispersion relation to lowest order in $k^2 v_A^2 / \Omega_0^2$ gives

$$\sigma^2 = \left[4 \left(\frac{\Omega_0}{\kappa} \right)^2 - 1 \right] k^2 v_A^2. \quad (11)$$

Suppose that a given mode can grow exponentially for a time τ before it is truncated by mode coupling or some other unspecified physical process. Then, the slowest growing mode that actually experiences significant growth (hereafter, the slowest appreciably growing mode [SAGM]) has $\sigma_{sagm} = 2\pi/\tau$ and a wavenumber given by

$$k_{sagm}^2 v_A^2 = \frac{4\pi^2 \kappa^2}{\tau^2 (4\Omega_0^2 - \kappa^2)}. \quad (12)$$

Our hypothesis is that the transition point in the flux-stress relation corresponds to the point where the slowest appreciably growing mode is just resolvable, i.e., where $\lambda_{sagm} \equiv 2\pi/k_{sagm} \sim 8\Delta$. This predicts a transition point at

$$\lambda_{MRI} \sim \frac{16\kappa}{15^{1.2}\pi(4\Omega_0^2 - \kappa^2)^{1/2}} \frac{\Delta}{\tau'}, \quad (13)$$

where $\tau' \equiv \tau/t_{orb}$, t_{orb} being the orbital period at that radius.

Equation 13 offers some insight into the transition point found in the flux-stress relations that we have been considering. In the local unstratified simulations of Pessah et al. (2007), the implicit potential is Newtonian ($\kappa^2 = \Omega_0^2$) and we find that $\lambda_{MRI} \sim \Delta$, implying $\tau \sim t_{orb}$. In the global simulations presented here, we find the transition point at $\lambda_{MRI} \sim \Delta/20$ which (accounting for the fact that $\kappa^2 < \Omega_0^2$ in the pseudo-Newtonian potential) gives $\tau \sim 5 - 10t_{orb}$. Thus, within the framework of this argument, the difference in the location of the transition point between the local unstratified and the global simulations is due to a difference in the robustness of the long wavelength and slowly growing modes; slowing growing modes appear to be able to grow for longer within the global simulation before being truncated. The nature of this difference, which must be closely related to the saturation of the turbulent state,

is beyond the scope of this paper and will be explored in future work.

3.4. Temporal correlations in flux-stress

The results of §3.2 suggests that the (fluctuating) magnetic flux threading a local patch of the disk determines the $r - \phi$ component of the magnetic stress generated by the turbulence in that patch. If the vertical magnetic flux is indeed the causal agent in determining the stress, we expect a temporal lag between fluctuations in the magnetic flux and the resulting variations in the stress. On the basis of experiments with local simulations (Hawley et al. 1996), we expect this lag to be approximately two (local) orbital periods. Thus, we expect the temporal lag to increase with radius in the disk due to the increasing orbital period.

To search for this lag, we use `Thin.M-Res.6z` and output the 3-d structure of the disk once every 0.1 ISCO orbits during the interval between 50–90 ISCO orbits (this is 10 times the nominal data output rate). Using these 400 snapshots of the disk structure, we then computed the instantaneous vertical magnetic fluxes and magnetic $r - \phi$ stresses in families of co-moving wedges at three radii $r \in \{8r_g, 10r_g, 12r_g\}$. The azimuthally averaged value of v_ϕ at each radius was used to track a given co-moving wedge between timesteps. This procedure is not fully lagrangian, because it does not account for the radial movement or fluctuating azimuthal velocity of a co-moving patch, but we expect these effects to be negligible for the short timeframe under consideration. The time-series of magnetic flux and stress for each wedge were then cross-correlated and, finally, the cross-correlations for all wedges at a given radius were averaged.

The resulting averaged temporal cross-correlations are shown in Fig. 4. At each radius we see a strong instantaneous correlation, likely due to the immediate shearing of perturbed vertical fields. However, in general, the cross-correlation is biased toward positive lag. This is consistent with what we would expect, namely that the presence of vertical flux will feed the MRI and result in enhanced transport. Of note is the fact that the inner-most radius considered, $R = 8r_g$ exhibits a double peak structure whereas this is unresolved at higher radii. Also peculiar is the fact that the outer-most radius, $R = 12r_g$ is significantly less biased towards positive lag than the other radii under consideration. A further exploration of these issues is beyond the scope of this paper, and will be explored in future work employing orbital advection algorithms and test-particle tracers in order to correctly follow the evolution of a local patch.

3.5. The dependence of stress on vertical domain size

When considering the correlation between vertical flux and stress we work directly with $M_{r\phi}$, but when studying possible trends in average stress with domain size we instead define an effective α -parameter (Shakura & Sunyaev 1973). For each snapshot we define a density-weighted spatial average via,

$$\alpha_M = \left\langle \frac{\int -\frac{\rho M_{r\phi}}{p} dz}{\int \rho dz} \right\rangle_{\phi, r \in (7r_g, 12r_g)}. \quad (14)$$

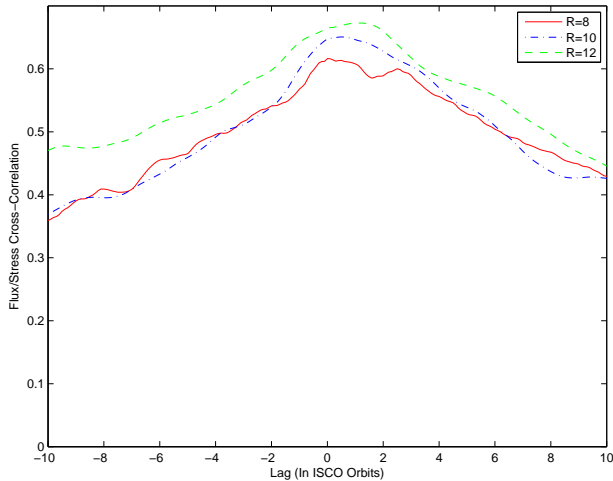


FIG. 4.— Cross-correlation of flux and stress evaluated in co-moving patches of the disk. Positive lags imply that changes in the vertical flux occur, on average, prior to changes in the magnetic stress.

The restriction on the radial range of the averaging is designed to ignore the plunging region of the accretion flow ($r \lesssim 6r_g$) and any effects related to the outer radial boundary. Density weighting is used in the vertical direction to take into account the low density, highly magnetized regions while still allowing the dominant contribution to the integral to come from the denser mid-plane of the disk.

A comparison of α_M and its dependence on vertical domain is given in Figure 5. The initial growth phase of the MRI is unaffected by the vertical domain as expected, since all the simulations considered have the same vertical resolution and can thus resolve the same unstable MRI modes. Over the course of the simulations, the larger vertical extent simulations have, in general, larger values of α_M . We attribute this effect to stifling of the growth of the magnetized regions in the smaller vertical extent simulation. However, the long-term effects of vertical extent are ambiguous. Whether the simulations converge to the same α_M or the apparent convergence is a result of short-term variability is unclear from the current simulations. Longer simulations will need to be carried out to determine the vertical domain size that is needed in order to reliably capture the dynamics of a global disk.

3.6. Long term behavior

In the one case of run `Thin.M-Res.6z`, the disk was simulated for 664 ISCO orbits. This simulation allows us to search for long-term trends in the dynamics of the disk. As shown in Figure 6 there is a slight downward drift in α_M over time. The same temporal trend is also evident in the flux-stress relationship. Figure 7 shows the flux-stress relationship averaged in 100 orbit blocks starting at 50 ISCO orbits. During the first 300 orbits, there appears to be a secular drift in the flux-stress relation. The linear (high-flux) part of the relation achieves a steady state relatively quickly (only the first time block between 50 and 150 ISCO orbits shows significant differences), but the flat (low-flux) part of the relation continues to fall until it too achieves a steady state at approximately 350 ISCO orbits into the run. Associated

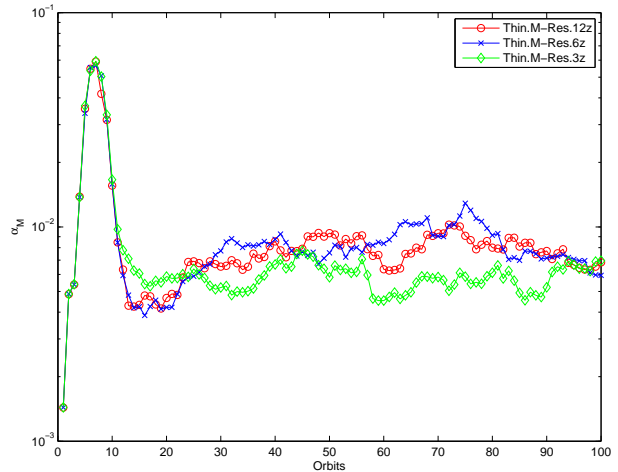


FIG. 5.— Behavior of α_M and its dependence on vertical domain.

with this, the “knee” in the flux-stress relation appears to move to smaller fluxes.

In essence, this result says that low-flux regions still support (small) stresses at early times but that those stresses decay over a period of several hundred ISCO orbits. We ascribe this to stresses associated with a sheared residual of the initial magnetic field configuration which are “mixed away” on a relatively long timescale. Our initial field configuration threads the midplane with regions of net magnetic flux which alternate with a radial periodicity of $5h$. Radial Fourier transforms of the mid-plane azimuthally-averaged B_z do indeed find a (weak) periodicity corresponding to the initial field even once the turbulence is fully developed. This periodic component grows weaker and is no longer detectable at approximately the same time that the flux-stress curve achieves steady-state. These observations further suggest that residual flux from the initial conditions is responsible for the long term variability.

Assuming that a long-lived residual of the initial magnetic field is the driving mechanism for this phenomenon, we can recover the time required to achieve the steady state from elementary arguments. The time needed to turbulently diffuse together two patches of oppositely directed flux separated by a radial distance $\Delta r = 2.5h$ is given by

$$t_{\text{mix}} \sim \frac{\Delta r^2}{\eta_{\text{eff}}}, \quad (15)$$

where η_{eff} is the effective turbulent resistivity. If we define $Pr_{\text{m,eff}}$ as the effective turbulent magnetic Prandtl number (i.e. the ratio of the effective turbulent viscosity to the effective turbulent resistivity), we can write

$$\eta_{\text{eff}} = Pr_{\text{m,eff}}^{-1} \alpha_M c_s h, \quad (16)$$

where c_s is the sound speed. We can then write the mixing time as

$$t_{\text{mix}} \sim \frac{Pr_{\text{m,eff}}}{2\pi\alpha_M} \left(\frac{\Delta r}{h}\right)^2 t_{\text{orb}}, \quad (17)$$

where t_{orb} is the local orbital period and we have used the fact that $h/c_s \sim r/v_\phi \sim t_{\text{orb}}/2\pi$. Using $Pr_{\text{m,eff}} = 1$ (Guan & Gammie 2009; Lesur & Longaretti

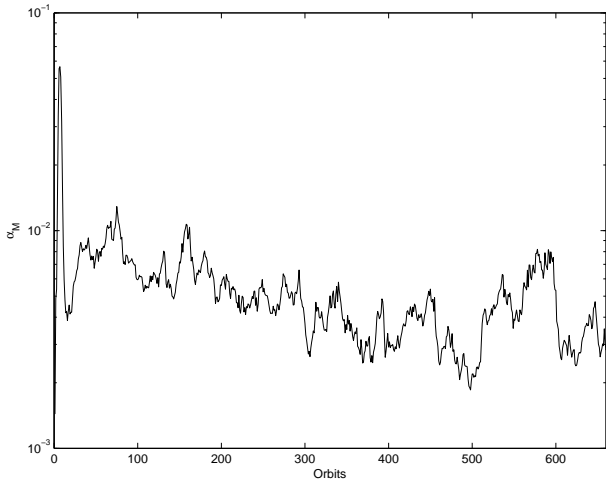


FIG. 6.— Long term behavior of α_M for run **Thin.M-Res.6z**.

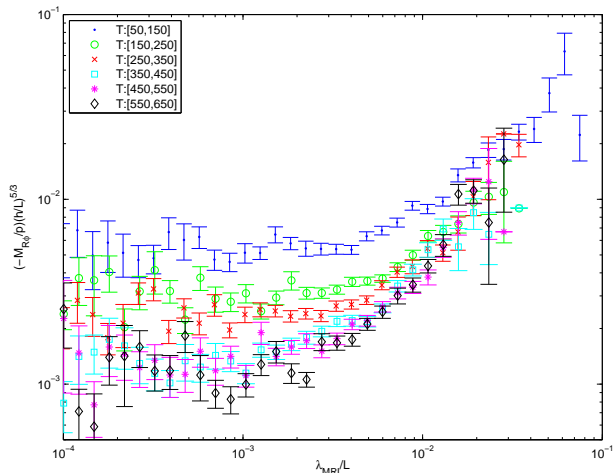


FIG. 7.— Flux versus stress averaged over 100 orbit blocks for run **Thin.M-Res.6z**. Vertical centering of $z = h$.

2009; Fromang & Stone 2009) and $\alpha_M = 0.005$ suggests that the memory of the initial conditions will be lost on a timescale of $t_{\text{mix}} \sim 200t_{\text{orb}}$. This crude estimate is in reasonable agreement with the timescale on which we see the flux-stress relationship achieve a stationary state.

4. CONCLUSIONS

It has been a long-held ansatz that one can extract and model the dynamics of a local patch of an accretion disk and obtain results (for the angular momentum transport, for example) that have meaning for the disk as a whole. By examining local patches of a high resolution global disk simulation, we have provided a direct test of this notion. We have shown that MRI-driven turbulence in global geometrically thin accretion disks behaves in a way consistent with scaling laws derived for local simulations. In particular, we find that global disks display a local flux-stress relation qualitatively similar to that found in local simulations (Hawley et al. 1995; Pessah et al. 2007). However, other aspects of the global models are distinctly different:

1. Even though we model a global accretion disk that has zero net magnetic field, any given patch of the disk is threaded by a net magnetic flux resulting from the self-generated field in the MRI-dynamo. Across much of the disk, the local flux is strong enough to have a controlling effect on the local stress. Thus, our *zero-net field* global disk is behaving as a collection of *net field* local patches.
2. The normalization, slope, and location of the “knee” of the flux-stress relationship changes with vertical height in the accretion disk. This amplifies the role of the off-midplane region ($h < |z| < 2h$) of the disk; not only does this region have stronger vertical magnetic fields than the midplane, but a given vertical field induces stronger magnetic stresses. The result is a strong enhancement of magnetic stress well off the midplane of the disk.
3. The transition point (or “knee”) in the flux-stress relation occurs as significantly smaller fluxes in the global simulation as compared to the local unstratified simulations. We relate this transition point to the ability of the simulation to marginally resolved the slowest appreciably growing mode.
4. Angular momentum transport (i.e. α_M) in the global disk appears to be impeded if the vertical domain size of the simulation is too small; we found significant differences between our $z = \pm 5h$ and $z = \pm 10h$ cases. On the other hand, the $z = \pm 10h$ and $z = \pm 20h$ cases appear very similar suggesting convergence has been achieved. Given that magnetic linkages between different patches of the disk appear to be crucial for determining the local flux (and hence the local stress), and that such linkages are made through the low-density corona of the disk, such a sensitivity to the vertical domain size is not surprising.
5. Analysis of our long simulation (which ran for 664 ISCO orbits) reveals long-term secular trends. In particular, there is a secular drift of the flux-stress relationship such that the knee of the relationship moves to smaller fluxes and the low-flux normalization decreases. This secular drift stabilizes after approximately 300 ISCO orbits. We attribute this to stresses associated with a long-lived residual of the initial magnetic field configuration.

We would like to thank Cole Miller, Sean O’Neill, Aaron Skinner, Eve Ostriker, and Jim Stone for valuable discussions and comments, and the Isaac Newton Institute for Mathematical Sciences for their hospitality during the completion of this work. K.A.S. thanks the Maryland-Goddard Joint Space Science Institute (JSI) for support under their JSI graduate fellowship program. K.A.S. and C.S.R. gratefully acknowledge support by the National Science Foundation under grant AST-0607428. P.J.A. acknowledges support from the NSF (AST-0807471), from NASA’s Origins of Solar Systems program (NNX09AB90G), and from NASA’s Astrophysics Theory program (NNX07AH08G).

REFERENCES

Balbus, S. A., & Hawley, J. F. 1991, *ApJ*, 376, 214

—. 1998, *Reviews of Modern Physics*, 70, 1

- Bodo, G., Mignone, A., Cattaneo, F., Rossi, P., & Ferrari, A. 2008, *A&A*, 487, 1
- Brandenburg, A., Nordlund, A., Stein, R. F., & Torkelsson, U. 1995, *ApJ*, 446, 741
- Davis, S. W., Stone, J. M., & Pessah, M. E. 2009, *ApJ*, submitted (arXiv:0909.1570)
- Fromang, S., & Nelson, R. P. 2006, *A&A*, 457, 343
- Fromang, S., & Stone, J. M. 2009, *A&A*, 507, 19
- Guan, X., & Gammie, C. F. 2009, *ApJ*, 697, 1901
- Guan, X., Gammie, C. F., Simon, J. B., & Johnson, B. M. 2009, *ApJ*, 694, 1010
- Hawley, J. F., Gammie, C. F., & Balbus, S. A. 1995, *ApJ*, 440, 742
- . 1996, *ApJ*, 464, 690
- Hayes, J. C., Norman, M. L., Fiedler, R. A., Bordner, J. O., Li, P. S., Clark, S. E., ud-Doula, A., & Mac Low, M.-M. 2006, *ApJS*, 165, 188
- Johansen, A., Youdin, A., & Klahr, H. 2009, *ApJ*, 697, 1269
- Lesur, G., & Longaretti, P. 2009, *A&A*, 504, 309
- Miller, K. A., & Stone, J. M. 2000, *ApJ*, 534, 398
- Paczynski, B., & Wiita, P. J. 1980, *A&A*, 88, 23
- Pessah, M. E., Chan, C.-k., & Psaltis, D. 2007, *ApJ*, 668, L51
- Regev, O., & Umurhan, O. M. 2008, *A&A*, 481, 21
- Reynolds, C. S., & Miller, M. C. 2009, *ApJ*, 692, 869
- Sano, T., Inutsuka, S., Turner, N. J., & Stone, J. M. 2004, *ApJ*, 605, 321
- Shakura, N. I., & Sunyaev, R. A. 1973, *A&A*, 24, 337
- Spruit, H. C., & Uzdensky, D. A. 2005, *ApJ*, 629, 960
- Stone, J. M., & Norman, M. L. 1992, *Astrophysical Journal, Supplement*, 80, 753